NeuroImage: Clinical 24 (2019) 102072

Contents lists available at ScienceDirect

NeuroImage: Clinical

journal homepage: www.elsevier.com/locate/ynicl

Focal epilepsy caused by single cerebral cavernous malformation (CCM) is associated with regional and global resting state functional connectivity (FC) disruption

Jason D'Cruz[a,1], Matthew Hefner[a,1], Christina Ledbetter[a,1], Clifton Frilot[b], Brady Howard[a], Peimin Zhu[c], Rosario Riel-Romero[c], Christina Notarianni[a], Eduardo Gonzalez Toledo[d], Anil Nanda[e], Hai Sun[a,*]

[a] Department of Neurosurgery, Louisiana State Unversity Health Science Center, Shreveport, LA 71103, United States
[b] School of Allied Health Professions, Department of Rehabilitation Sciences, Louisiana State Unversity Health Science Center, Shreveport, LA 71103, United States
[c] Department of Neurology, Louisiana State Unversity Health Science Center, Shreveport, LA 71103, United States
[d] Department of Radiology, Louisiana State Unversity Health Science Center, Shreveport, LA 71103, United States
[e] Department of Neurosurgery, Robert Wood Johnson Medical School, New Brunswick, NJ 08903, United States

ARTICLE INFO

Keywords:
Focal epilepsy
Functional connectivity
Cerebral cavernous malformation
Resting state functional MRI
Default mode network
Epileptogenic zone
Brain connectomics

ABSTRACT

Epilepsy, including the type with focal onset, is increasingly viewed as a disorder of the brain network. Here we employed the functional connectivity (FC) metrics estimated from the resting state functional MRI (rsfMRI) to investigate the changes of brain network associated with focal epilepsy caused by single cerebral cavernous malformation (CCM). Eight CCM subjects and 21 age and gender matched controls were enrolled in the study. Seven of 8 CCM subjects underwent surgical resection of the CCM and became seizure free and 4 of the surgical subjects underwent a repeat rsfMRI study. We showed that there was both regional and global disruption of the FC values among the CCM subjects including decreased in homotopic FC (HFC) and global FC (GFC) in the regions of interest (ROIs) where the CCMs were located. There was also the disruption of the default mode network (DMN) especially the FC between the middle prefrontal cortex (MPFC) and the right lateral parietal cortex (LPR) among these individuals. We observed the trend of alleviation of these disruptions after the individual has become seizure free from the surgical resection of the CCM. Using a voxel-based approach, we found the disruption of the HFC and GFC in the brain tissue immediately adjacent to the CCM and the severity of the disruption appeared inversely proportional to the distance of the brain tissue to the lesion. Our findings confirm the disruption of normal brain networks from focal epilepsy, a process that may be reversible with successful surgical treatments rendering patients seizure free. Some voxel-based metrics may help identify the epileptogenic zone and guide the surgical resection.

1. Introduction

Cerebral cavernous malformations (CCM) are discrete vascular lesions that lack neuronal tissue and parenchyma but are peripherally surrounded by a pseudocapsule of gliotic brain tissue. These pseudocapsules generally contain hemosiderin deposits, which are the result of minor hemorrhage (Dillon, 1997; Robinson et al., 1991; Sze et al., 1987). Patients with CCMs frequently develop seizure disorders, which are most often focal in nature. Many will, however, secondarily generalize and are often refractory to medical management (Simard et al., 1986). It is presumed that in CCM-related epilepsy, seizure activity originates from the hemosiderin-laden cortex surrounding the lesion. This phenomenon is largely due to the fact that the lesions themselves do not contain neural tissue, and hemosiderin deposits are known to be highly epileptogenic (Steiger et al., 1987). Structural brain lesions such as CCM are considered to be the center of epileptogenic zone (Bernasconi, 2017), and the removal of such lesion and the surrounding abnormal brain has a high success rate of rendering patients seizure free (de Tisi et al., 2011; Jette and Wiebe, 2013; Mohammed et al., 2012; Spencer et al., 2005; Wiebe, 2012). An increasing body of evidence suggests that seizures result not only from alterations in excitability in the epileptogenic zone but also abnormalities in neuronal networks

* Corresponding author.
E-mail address: hai.sun@rutgers.edu (H. Sun).
[1] Those authors contributed equally to this work.

https://doi.org/10.1016/j.nicl.2019.102072
Received 12 September 2019; Received in revised form 9 October 2019; Accepted 4 November 2019
Available online 05 November 2019

(Bernhardt et al., 2013; Kramer and Cash, 2012). These network abnormalities leading to seizures can range from local circuits within an epileptogenic structure to connections involving the entire brain (Englot et al., 2016). These new understandings challenge the traditional concept of "focal epilepsy." Focal epilepsy associated with a single CCM is an excellent pathology to study the impact of an epileptogenic structure on the entire brain network.

Two variants of standard MRI technique have been utilized to characterize network abnormalities associated with seizure disorders. Diffusion weighted MRI infers structural connectivity by identifying white matter fibers that physically connect two brain regions (Hagmann et al., 2003; Le Bihan et al., 2001). Conversely, resting state functional MRI (rsfMRI) estimates functional connectivity (FC) among brain areas from correlations of blood oxygen level dependent (BOLD) signals (Biswal et al., 1995; Lowe et al., 2000; van den Heuvel and Hulshoff Pol, 2010).

While resting state connectivity disturbances have been investigated and identified in both generalized and focal epilepsy (Bernhardt et al., 2013; Christiaen et al., 2019; Englot et al., 2016; Grassia et al., 2018; Liao et al., 2010; Moeller et al., 2011; Pittau et al., 2012), no studies to date have specifically focused on drug resistant CCM-related epilepsy. Here, we study the impact of CCM-associated epilepsy on functional connectivity by analyzing rsfMRI data acquired from subjects before and after surgical resection of the epilepsy focus. In order to fully characterize the impact of CCM on various brain networks, we utilized a multi-resolution approach to study the alteration of several FC metrics among the participants. This multi-resolution approach, in turn, allows us to investigate the alteration of brain connectomics at local, regional, and global levels.

2. Methods

2.1. Study design

A retrospective chart review was conducted to identify subjects with single CCM and seizure disorders between September 2015 to June 2019. We have also recruited age- and gender-matched control subjects for this study. Informed consent to participate in this Louisiana State University Health Science Center (LSUHSC) Institutional Review Board (IRB) approved study was obtained for both the CCM and control subjects. All CCM subjects had undergone extensive work up as a part of surgical treatment of their seizure disorder. The workup included presurgical video electroencephalogram (vEEG), presurgical MRI studies of the brain, and neuropsychological testing. The preoperative MRI studies including anatomical and resting state functional MRI sequences. All patients' vEEG recordings suggested that the region of a single CCM is likely involved in the epileptogenic zone (EZ). The surgical resection of the CCM and its surrounding EZ was recommended. After the surgical resection, patients were evaluated with regular follow up visits. Postoperative MRI studies were obtained as a part of follow up using the same imaging protocols. Each control subject reported no history of neurological or psychological diseases, suffered no head trauma and underwent no prior neurosurgical procedures. The control subjects underwent the imaging data acquisition with the same protocol.

The imaging studies obtained from both CCM and control subjects formed three groups. Group 1 consisted of MRI studies obtained from all CCM subjects before they underwent surgical resection of the CCM, i.e. the CCM pre-resection group. Group 2 consisted of all MRI studies obtained from a subset of CCM subjects after they have undergone surgical resection of the CCM, i.e., the CCM post-resection group. Group 3 consisted of all MRI studies obtained from the control subjects.

2.2. Imaging acquisition parameters

The MRI studies were acquired as part of the surgical epilepsy workup. All scans were performed on a 3 T (3T) Philips Ingenia MR system using a dStream HeadSpine 15-channel receive head coil. The acquisition protocol was standardized across subjects and included a T1-weighted anatomic scan as well as an echo planar imaging blood oxygen level dependent (EPI-BOLD) rsfMRI scan. Anatomical imaging was performed with the following parameters: 3D sagittal acquisition with 1 mm isotropic resolution, TR 7.5 ms, TE 3.5 ms, and reconstruction to a 240×240 image matrix. Functional imaging was performed with the following parameters: 140 dynamic acquisitions, slice thickness 5 mm, TR 2000 ms, TE 35 ms, and reconstructed to a 144×144 image matrix. Control subject studies were acquired with an identical imaging protocol.

2.3. Imaging data pre-processing

For all subjects, preprocessing and connectivity analyses were performed using SPM 12 software (statistical parametric mapping, https://www.fil.ion.ucl.ac.uk/spm/doc/spmbib.html), version17 of the CONN toolbox (Whitfield-Gabrieli and Nieto-Castanon 2012; www.nitrc.org/projects/conn), AFNI(Cox, 1996), and custom MATLAB (the Mathworks, Inc. Natick, MA, USA) scripts. The preprocessing steps performed using the CONN toolbox included (1) functional realignment to correct for head movement and movement distortion, (2) scrubbing, (3) co-registration of the EPI to subjects' T1 anatomical image, (4) functional segmentation and normalization to the Montreal Neurological Institute (MNI) template, (5) structural segmentation and normalization to the MNI template, and (6) spatial smoothing with an 8 mm full width and half-maximum (FWHM) Gaussian kernel. Next, we performed linear and quadratic detrending of the fMRI signal, covarying out white matter (WM) and cerebrospinal fluid (CSF) signal, and regression of motion parameters and their first derivatives. WM and CSF signals were estimated for each volume by thresholding the SPM tissue probability maps. The resting data were then bandpass-filtered.

After preprocessing, AFNI was used to mask each subject's functional dataset. From each subject's anatomical image, the voxels contained within the CCM were manually identified, and a mask to remove gray matter voxels was created. These masks were then applied to the resting state functional datasets such that the connectivity analyses would not include aberrant signals from within the CCM.

2.4. Multi-resolution analyses

In this study, the resting state data was processed using seed methods (Andrews-Hanna et al., 2007; Biswal et al., 1995; Cordes et al., 2000; Fransson, 2005; Larson-Prior et al., 2009). Our seeds were defined in two different resolutions: a region of interest (ROI)-based analysis and a voxel-based analysis.

A ROI-based analysis was performed using the CONN toolbox. Within CONN toolbox, each subject's T1 anatomical images were first spatially normalized to the common MNI atlas then segmented into 136 ROIs defined by the atlas. Segmentation was then applied to the masked resting state functional datasets. The resting state BOLD time series of any given ROI was estimated by averaging the BOLD time series across all grey matter voxels in the ROI. The Fischer z-transformation was calculated from the correlation coefficients between each ROI to ROI BOLD time series pair resulting in a 136×136 connectivity matrix. The ROI to ROI connectivity matrices for all subjects were exported from the CONN toolbox for statistical analysis. Specifically, ROI to ROI connectivity was used to access the homotropic connectivity, global connectivity and DMN connectivity metrics, which will be defined in the following section.

The voxel-based analysis, however, utilized the resting state BOLD time series of each voxel for computing the FC metrics between two voxels. Using the voxel-based analysis, we examined the changes in the FC metrics in the tissue surrounding the CCM lesion. Here we investigated whether the epileptogenic zone surrounding the CCM is associated with the alteration in their FC values. To do so, we used the

CONN toolbox and custom MATLAB scripts. Resting state time series image data was exported from the CONN toolbox into MATLAB. Within MATLAB, the area surrounding the CCM lesion was defined as three rings radiating outward from the CCM, each ring being one voxel wide (2 mm). The rings were named serially in order of increasing distance away from the lesion, with ring 1 immediately surrounding the lesion, and ring 3 being the farthest away from the lesion. For the controls, the congruent voxels within the MNI atlas template were used to define the rings. The CCM post-resection group was not considered for voxel to the voxel-based analysis, as the alteration in brain parenchyma post-resection of the lesion did not permit us to accurately define the region surrounding the resected CCM lesion. We investigated the changes in FC metrics associated with the CCM-related focal epilepsy in both macro- (ROI-based) and micro- (voxel-based) scopic scales using this multi-resolution approach.

2.5. The functional connectivity (FC) metrics

The functional connectivity (FC) was examined across the three imaging study groups. The central hypothesis was that the FC metrics are altered in patients with CCM at both regional and global network levels. To test this hypothesis, we compared the FC metrics estimated among CCM pre-resection group with those estimated from the age- and gender-matched control group. Furthermore, we investigate whether the surgical resection rendering patients seizure free may change for the FC in the brain for these individuals. To do so, we estimated the changes in same regional and global FC metrics among CCM subjects before and after resection. The following regional and global FC metrics were included in the comparison. All FC metrics were estimated by first computing Pearson's correlation coefficient between two resting state time series being considered. In the ROI-based analysis, the resting state time series was the average of all time-series of all grey matter voxels in the ROI. In the voxel-based analysis, the resting state time series was the time series of the voxel of interest. The final FC value is cast as the z-score of the Pearson's correlation coefficient. Conventionally, if z-score is greater than 0.424 (corresponding to Pearson's correlation coefficient of 0.4), the FC is deemed significant.

1 The homotopic FC (HFC)

Functional homotopy, the high degree of synchrony in spontaneous activity between geometrically corresponding interhemispheric (i.e. homotopic) regions, is a fundamental characteristic of the intrinsic functional architecture of the brain. This high level of correlated activity between the left and right hemispheres have long been demonstrated by electrophysiological studies (Aboitiz et al., 2003; Duffy et al., 1996). This symmetry is also reflected by FC metrics obtained from resting state FC. Studies have shown there is robust homotopic resting state FC (Salvador et al., 2007; Stark et al., 2008), an unsurprising finding given the high proportion of callosal fibers dedicated to homotopic connectivity (Innocenti et al., 1995).

Using a ROI-based approach, we assessed the homotopic FC (HFC) between the ROI associated with CCM lesion and the homotopic ROI contralateral to it. For the hemisphere in which a CCM lesion was located, the data was masked such that the averaged signal did not include the signal measured within the CCM lesion itself. The HFC was quantified as z-score of the Pearson's correlation coefficient of the BOLD time series between the two homotopic ROIs involving the CCM lesions. The HFC was then compared to the HFCs (also z-scores) estimated from the same ROIs estimated among the age- and gender-matched control groups.

Using the voxel-based analysis, we examined the changes of HFC in the tissue surrounding the CCM lesion. The HFC of each voxel is defined as z-score of the Pearson's correlation coefficient for the resting state time series between this voxel and its homotopic paired voxel. The HFC of each ring was then estimated by averaging of the HFC of all grey matter voxels within each ring. The HFCs of each of the three rings of the CCM pre-resection group was compared to the HFCs of the corresponding ring of the age- and gender-matched control group using a single factor ANOVA test.

1 The global FC (GFC)

The impact of the focal epilepsy is not limited to the region where the epileptogenic zone is located. The impact of the focal seizure on global brain networks is reflected by the fact that patients with focal epilepsy were more likely to have cognitive and neuropsychological deficits compared to individuals without seizures (Verche et al., 2018; Zhang et al., 2018). To assess the global brain network changes associated with CCM-induced focal epilepsy, we used the global FC (GFC) to assess the alterations of global brain networks. In the ROI-based analysis, we first computed the BOLD time series for each ROI by averaging the BOLD time series across all grey matter voxels within the ROI. The Fischer z-transformations (z-scores) were calculated from the Pearson's correlation coefficients between each ROI to ROI BOLD time series pair resulting in a 136×136 connectivity matrix. For each ROI, the row (or column) of the connectivity matrix associated with the ROI was inspected. The GFC of this ROI is defined as the number of elements in the row with absolute z-scores greater than 0.424 (corresponding to Pearson's correlation of 0.4), i.e., when the FC between the two ROIs was significant. The GFC of the ROI associated with the CCM is denoted as $GFC_{ipsilateral}$. The GFC for the homotopic ROI contralaterally to the CCM-associated ROI was calculated and denoted as $GFC_{contralateral}$. In order to compare the GFC of the affected ROI to the relatively unaffected homotopic contralateral ROI, we established a metrics defined as Relative GFC (RGFC). RGFC for each CCM ROI ($RGFC_{ROI}$) was calculated as shown by the formula below:

$$RGFC_{ROI} = FC_{contralateral}/GFC_{ipsilateral}$$

The RGC_{ROI} of the CCM pre-resection and CCM post-resection groups were each individually compared to the RGC_{ROI} of the congruent ROIs of the control group using a single factor ANOVA test.

We also investigated the changes of the GFC in the brain tissue surrounding the CCM in a microscopic scale using the voxel-based analysis. For the RGFC analysis, the GFC for voxels within each ring and the whole brain grey matter voxels were calculated. In addition, the correlation between the resting state time series of each voxel to the whole brain was calculated. Similar to the voxel-based analysis applied to the homotopic FC metric, we employed the CONN toolbox and custom MATLAB scripts. The area surrounding the CCM lesion was defined as three rings radiating outward from the CCM, similar to the voxel-based analysis for the HFC. For the controls, the congruent voxels within the MNI atlas template were used to define the rings. Similar to the ROI-based approach, the GFC of a voxel is defined as the number of voxels with significant FC with the voxel of interest. $GFC_{ipsilateral}$ and $GFC_{contralateral}$ are then defined and computed similar to the ROI-based analysis for the GFC but using the number of voxels rather than the number of ROIs. The RGFC for each voxel ($RGFC_{voxel}$) was calculated as shown by the formula below:

$$RGFC_{voxel} = GFC_{contralateral}/GFC_{ipsilateral}$$

The $RGFC_{voxel}$ for each ring was calculated by averaging the $RGFC_{voxel}$ of all grey matter voxels of each ring. The $RGFC_{voxel}$ of each of three rings of the CCM pre-resection group was then compared to the $RGFC_{voxel}$ of the corresponding ring of the age and gender-matched control group using a single-factor ANOVA test.

1 The Default Mode Network FC (DFC)

The Default Mode Network (DMN) is a large scale brain network known to have highly correlated functional connectivity among its interacting regions (Buckner et al., 2008; Raichle et al., 2001;

Weaver et al., 2018). The DMN is believed to be composed of four major interacting regions of the brain (Gusnard et al., 2001). These include the middle prefrontal cortex (MPFC), the left lateral parietal cortex (LPL), the right lateral parietal cortex (LPR), and the posterior cingulate cortex (PCC) (Hamilton et al., 2015; Mulders et al., 2015). Diseases affecting the central nervous system also affect the connectivity among the DMN. To estimate the DMN FC (DFC), we used the MPFC, a midline ROI, as the seed in a ROI-based analysis. Similar to other ROI-based analyses described in the previous section, the resting state BOLD time series of all four DMN-related ROIs were estimated by averaging the BOLD time series across all grey matter voxels in each ROI. Next, the DFC was estimated as the Fischer z-transformation value between the BOLD time series of MPFC and the time series of each of the three other DMN nodes i.e., LPL, LPR, and PCC. Hence, each DFC consists of three Fisher z-transformation values. For statistical comparison, the DFC of the CCM pre-resection and CCM post-resection groups was compared to the age and gender-matched control group.

Furthermore, in order to examine the effect of laterality of the lesion on the DMN connectivity, we divided the CCM pre-resection group into 2 smaller subsets: the first group of subjects having lesions in the left cerebral hemisphere and the second group of subjects having lesions in the right cerebral hemisphere. We then conducted the same analysis by compared the DFC of these two CCM subject groups with the control group as described above.

2.6. Statistical analysis

As shown in Fig. 1, the location of CCM in the brain is diverse among the study participants. We defined the FC metrics to characterize changes in regional and global functional networks so that the estimated values can be compared between the CCM and control participants despite of the varying locations among the lesions. In this study, two types of hypothesis testings were conducted between the two participant groups. When the statistical comparison was to ask whether the values estimated from the CCM group were different from those from the control group, an ANOVA test was employed. When the statistical comparison was to ask whether the values estimated from the CCM group were either greater or less than those from the control group, a two-tailed *t*-test was used instead. A threshold of $p < 0.05$ was considered significant. The analyses were performed using custom MATLAB scripts.

3. Results

Eight subjects with single CCM and intractable epilepsy were identified between September 2015 and May 2019. Shown in Table 1

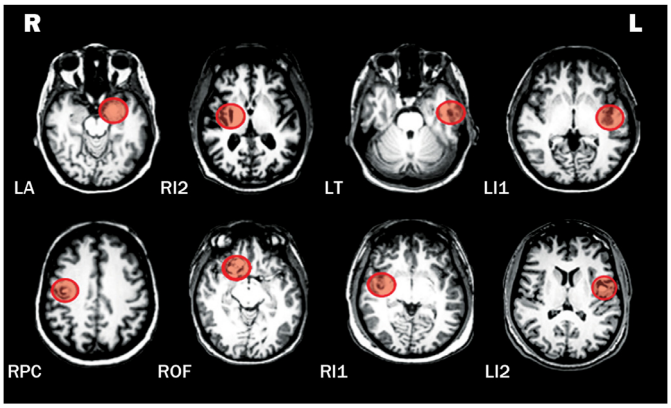

Fig. 1. The anatomical location of single CCM lesion among the study participants. Shown here are axial T1 anatomical scans of the 8 CCM subjects. The red circles indicate the CCM lesion. Each image is labelled with the subject identifier.

Tables 1
The demographics of the CCM subject. The subjects marked with asterisks (*) underwent repeat MRI study after the surgical resection of the CCM. RI2$^+$ is the subject who suffered ischemic cerebral infarction and the surgical resection of his CCM was postponed.

Subject	Age/Sex	CVM Location	CCM Volume (mm^3)
RI1*	17/M	Right insular cortex	428
RI2$^+$	48/M	Right insular cortex	5850
ROF	29/M	Right orbital frontal gyrus	5378
RPC	54/F	Right precentral gyrus	75
LT*	25/F	Left Posterior Inferior Temporal Gyrus	392
LI1*	50/F	Left insular cortex	1201
LI2	20/M	Left insular cortex	6102
LA*	66/F	Left amygdala	2327

are the demographics of these subjects and the volume of each CCM measured after the segmentation of the lesion from anatomical MRIs. The surgical work-up identified the region surrounding the CCM as the epileptogenic zone. All subjects except one had resection of the CCM as part of their treatment regimen. One CCM subject developed cerebral ischemic infarction prior to the scheduled surgical resection. The infarction involving left thalamus, basal ganglia and internal capsule resulted in significant weakness and disability requiring extensive rehabilitation. The epilepsy surgery was postponed. Among 7 CCM subjects who underwent surgical resection, none suffered postoperative complications and all remained seizure free at the latest follow up. The mean follow-up period of these 7 patients was 25.5 months (ranged between 5 and 37 months). Four subjects who had undergone surgical resection underwent postoperative MRI studies using the same acquisition protocols between 6 and 13 months (mean 7.8 months) after the resection of their CCM. T1-weighted anatomic images of the eight CCM subjects with the lesion highlighted are shown in Fig. 1. As evident in this figure, the location of the CCM varied among the subjects. We included 21 age- and gender-matched controls for this study, Table 2, and they underwent the MRI studies with the same imaging acquisition protocols.

We employed three FC metrics to investigate both regional and global FC changes associated with the CCM-related focal epilepsy, i.e., the homotopic, global, and default mode network (DMN) FCs. For both homotopic and (HFC) global (GFC) FCs, we performed both the ROI and voxel-based analyses. For the DMN FC (DHC), we employed the ROI-based analysis, and additionally asked whether the laterality of CCM location influenced the changes of the metric. Furthermore, in all the ROI-based analyses, we investigated whether these metrics changed after the CCM lesion has been resected and the subject became seizure free.

3.1. The homotopic FC (HFC)

1 The ROI-based Analysis

The homotopic FC (HFC) was quantified as the z-scores of the Pearson's correlation coefficient between the averaged BOLD time series in two homotopic ROIs. First, the HFCs were measured for the control group ($n = 21$). Of the 136 MNI ROIs, 116 ROIs form 58 homotopic pairs; therefore, it is possible to assess HFCs between these pairs. Among them, 49 were cerebral ROIs and 9 were cerebellar ROIs. Shown in Fig. 2 are the means and standard derivations (STDs) of HFCs

Table 2
The age and gender matched control group.

Characteristics	CCM subjects	Control subjects	P values
Age	37.1 (18–66)	35.6 (18–70)	0.48
Gender (M/F)	4/4	11/10	0.98

1	Frontal Pole	16	Inferior Temporal Gyrus, temporo-occipital	31	Temporal Fusiform Cortex, anterior division	46	Pallidum
2	Insular Cortex	17	Postcentral Gyrus	32	Temporal Fusiform Cortex, posterior division	47	Hippocampus
3	Superior Frontal Gyrus	18	Superior Parietal Lobule	33	Temporal Occipital Fusiform Cortex	48	Amygdala
4	Middle Frontal Gyrus	19	Supramarginal Gyrus, anterior division	34	Occipital Fusiform Gyrus	49	Accumbens
5	Inferior Frontal Gyrus, pars triangularis	20	Supramarginal Gyrus, posterior division	35	Frontal Operculum Cortex	50	Cerebellum Crus 1
6	Inferior Frontal Gyrus, pars opercularis	21	Angular Gyrus	36	Central Opercular Cortex	51	Cerebellum Crus 2
7	Precentral Gyrus	22	Lateral Occipital Cortex, superior division	37	Parietal Operculum Cortex	52	Cerebellum 3
8	Temporal Pole Right	23	Lateral Occipital Cortex, inferior division	38	Planum Polare	53	Cerebellum 4, 5
9	Superior Temporal Gyrus, anterior division	24	Intracalcarine Cortex	39	Heschl's Gyrus	54	Cerebellum 6
10	Superior Temporal Gyrus, posterior division	25	Paracingulate Gyrus	40	Planum Temporale	55	Cerebellum 7
11	Middle Temporal Gyrus, anterior division	26	Cuneal Cortex	41	Supracalcarine Cortex	56	Cerebellum 8
12	Middle Temporal Gyrus, posterior division	27	Frontal Orbital Cortex	42	Occipital Pole	57	Cerebellum 9
13	Middle Temporal Gyrus, temporo-occipital	28	Parahippocampal Gyrus, anterior division	43	Thalamus	58	Cerebellum 10
14	Inferior Temporal Gyrus, anterior division	29	Parahippocampal Gyrus, posterior division	44	Caudate		
15	Inferior Temporal Gyrus, posterior division	30	Lingual Gyrus	45	Putamen		

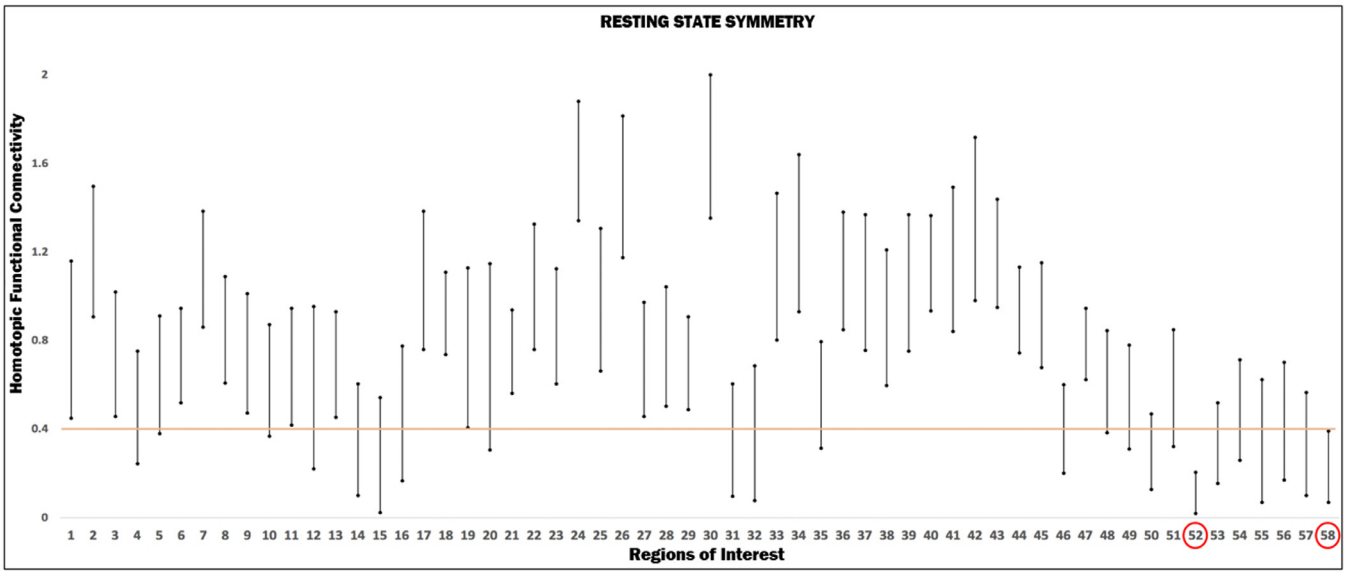

Fig. 2. The functional coactivation of the homotopic brain regions as measured in resting state connectivity among 21 health study participants. Forty eight of the 58 ROIs had the mean FC at least one standard derivation above the mean z-score if 0.424 (dotted line), which indicates significant FC. Only 2 regions (52 and 58, both located in cerebellum, red circle) had the mean FC one standard derivation below the dotted line.

among 58 homotopic pairs estimated from 21 control subjects. Forty-eight of the 58 ROIs had the mean FC at least one standard derivation above the mean z-score of 0.424, which indicates significant FC. Only 2 regions (52 and 58, both located in cerebellum) had the mean FC one standard derivation below 0.424. The functional coactivation of homotopic brain structures has been established by other studies (Stark et al., 2008; Toro et al., 2008). Our data from the control subject yielded similar findings.

The HFC was estimated for the CCM group pre-resection group (n = 8). For each subject within this group, the HFC of the ROI affected by the lesion was compared to the age and gender-matched control, Fig. 3 and Table 3. The HFC values of the lesional ROIs for 6 of the 8 CCM subjects was less than those of congruent ROIs for the age- and gender-matched controls. Although a two-tailed paired t-test to compare the HFC values between the controls and CCM group 'pre-resection' was not statistically significant (control: M = 0.94, SD = 0.35, CCM pre resection: M = 0.71, SD = 0.31; p = 0.12), the trend suggests the HFC was disrupted in CCM pre-resection group as compared to controls.

Table 4 and Fig. 4 show the comparison of the HFC between the controls, CCM pre resection group and the CCM post-resection group. Three out of 4 CCM subjects (RI1, LA and LI2) showed an increase in the HFC values after the resection while the HFC values for the other two subjects remained stable, Fig. 4. Although not statistically significant (p = 0.14, one-tailed t-test), the trend seems to suggest that surgical resection rendering seizure free may help recover the disruption of the HFC seen in the CCM subjects with focal epilepsy.

1 The voxel-based analysis

In order to analyze the changes in FC in the brain tissues surrounding the CCM, we performed the voxel-based analysis by dividing the region surrounding the CCM into three outward radiating rings of width equal to one voxel (2 mm). Shown in Table 5 and Fig. 5 are the comparison of the mean and STD of the HFC associated with each ring of brain tissues surrounding the CCM and the same anatomical rings identified in the control group. Although not statistically significant, the disruption of the HFC values was most severe in the ring immediately adjacent to the lesion and lessens as the rings move away from the lesion, Fig. 5 and Table 5.

3.2. The global FC (GFC)

1 The ROI-based analysis

Shown in Fig. 6 and Table 6 are the comparison of the GFC values among the ROIs where the CCMs were located ($GFC_{ipsilateral}$) and its contralateral homotopic ROIs ($GFC_{contralateral}$) and the GFC of the ROIs that corresponds to lesional ROIs in the control group. Note that the $GFC_{contralateral}$ values are closer to the mean of the GFCs estimated in the

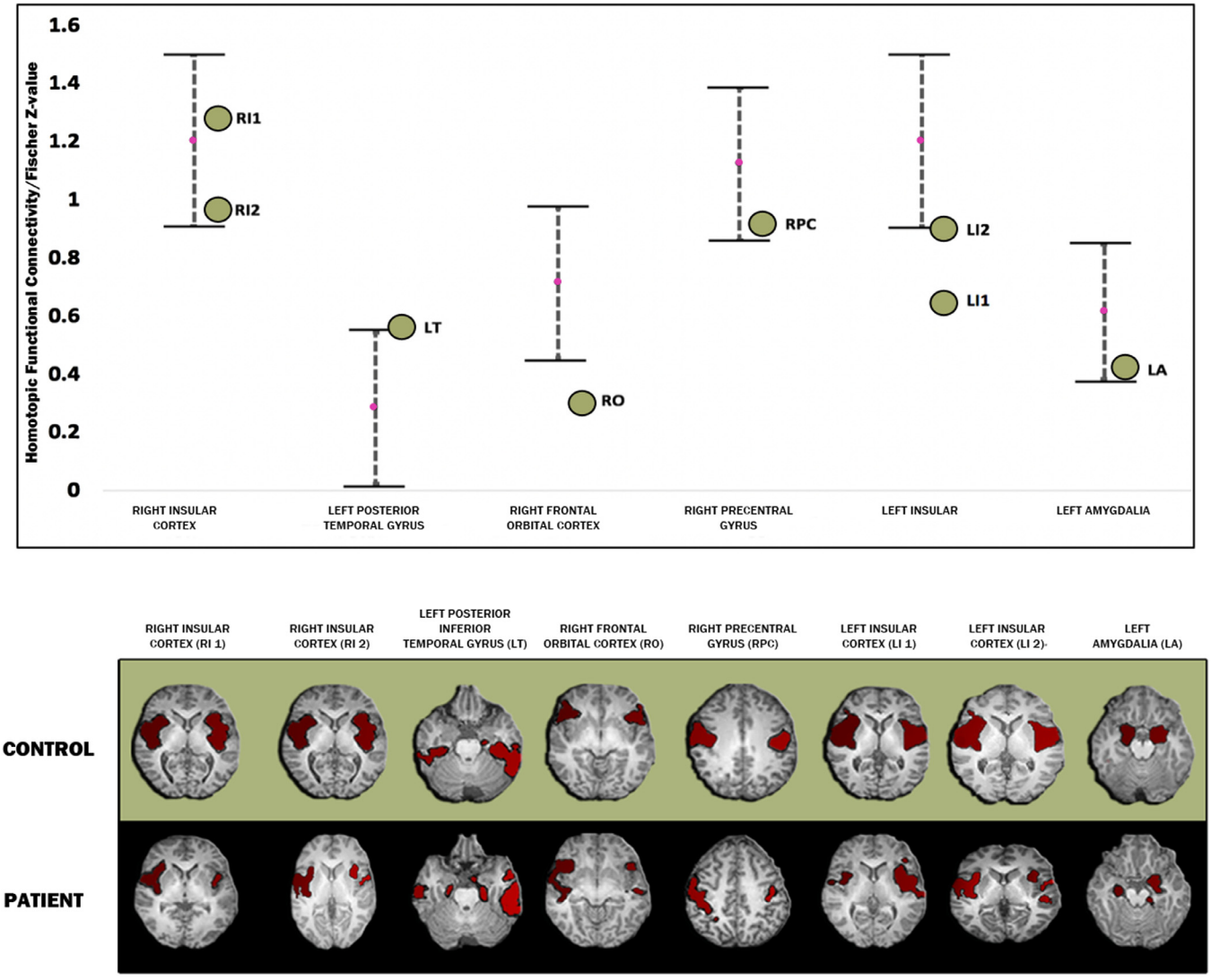

Fig. 3. Comparison of the homotopic FC (HFC) between the lesional ROIs and the same ROIs among the control subjects. The top plot shows the HFC of each ROI (circle, labelled with the subject identifier) overlaid on the mean and the standard derivation of the HFC of the corresponding ROI estimated from the age- and gender-matched controls (n = 21). Note that six of 8 CCM subjects had the HFC below the mean of HFC estimated for the same ROI from the control group. The bottom plot shows the coactivation maps for both the control (top row) and CCM (bottom row) subjects generated from the imaging processing software where the two voxels were marked red when they show BOLD time series coactivation. Note that the coactivation symmetry seen in the control group was disrupted in the CCM group, bottom row.

control group than the $GFC_{ipsilateral}$, Fig. 6. These findings suggested that, the GFCs associated with the lesional ROIs suffered more disruption than its homotopic counterparts. To quantitatively assess this change, we employed the metric, $RGFC_{ROI}$. Shown in Fig. 7 and Table 7 is the comparison of $RGFC_{ROI}$ among all subject groups. The $RGFC_{ROI}$ for each ROI is defined as the ratio between $GFC_{contralateral}$ and $GFC_{ipsilateral}$. The $RGFC_{ROI}$ of each ROI with the CCM are greater than the mean $RGFC_{ROI}$ of the corresponding ROI among the controls, which is close to 1, Fig. 7(A), and Table 7. Interestingly, the $RGFC_{ROI}$ value of the same ROI decreased after the CCM subject became seizure free after the surgical resection of the lesion, Fig. 7(A), and Table 7. While the increase of $RGFC_{ROI}$ (1.56 ± 0.45) among the CCM pre-resection group

Table 3
The comparison between the HFCs estimated from the CCM subjects in the ROIs associated with the CCM with those of the same ROIs estimated from the control subjects.

ROI associated with the CCM (subject)	HFCs from the CCM group	Mean/STD of HFCs from the same ROI among the control group
Right Insular Cortex (RI1)	1.19	1.20/0.29
Right Insular Cortex (RI2)	0.89	Same as above
Right Orbital Frontal Cortex (ROF)	0.27	0.71/0.26
Right Pre-central gyrus (RPC)	0.84	1.12/0.26
Left Posterior Inferior Temporal Gyrus (LT)	0.50	0.28/0.26
Left Insular Cortex (LI1)	0.60	1.20/0.29
Left Insular Cortex (LI2)	0.93	Same as above
Left Amygdala (LA)	0.38	0.61/0.23

Table 4
The comparison between the HFCs estimated from the CCM subjects in the ROIs associated with the CCM before and after the surgical resection.

ROI associated with the CCM (subject)	HFC before resection	HFC after resection	HFC among controls (mean/std)
Right Insular Cortex (RI1)	1.19	1.46	1.20/0.29
Left Posterior Inferior Temporal Gyrus (LT)	0.50	0.48	0.28/0.26
Left Insular Cortex (LI1)	0.6	0.46	1.20/0.29
Left Amygdala (LA)	0.38	0.6	0.61/0.23

relative to the $RGFC_{ROI}$ (0.98 ± 0.03) among the controls subjects was statistically significant ($p = 0.017$), the change of $RGFC_{ROI}$ among the 4 CCM subject between before and after surgery (0.83 ± 0.35) was not ($P = 0.2$), 7(B). Similar to the results with the HFC, our data suggested that the surgical resection rendering these subjects seizure free perhaps helped restore the GFC to its normalcy among these individuals.

1 The voxel-based analysis

In order to analyze the changes in GFC in the brain tissues surrounding the CCM, we performed the voxel-based analysis similar to the analysis carried out for the HFC. Shown in Fig. 8 and Table 8 are the comparison of the mean and STD of the $RGFC_{ROI}$ associated with each ring of brain tissues surrounding the CCM and the same anatomical rings identified in the control group. The $RGFC_{ROI}$ appears increased in the brain tissue surrounding the CCM lesion compared to the same tissue in the control group. Furthermore, although not statistically significant, the mean value associated with each ring seems to decrease as the ring becomes further away from the lesion, Fig. 8 and Table 8. Similar to the changes observed in the voxel-based analysis for the HFC, our data suggested that the CCM lesion disrupts the GFC associated with its surrounding brain tissue, and the disruption perhaps lessens as the distance between the brain tissue and lesion increases.

Table 5
The voxel-based analysis on the HFC changes in the surrounding brain tissue.

	Ring 1 (mean/std)	Ring 2 (mean/std)	Ring 3 (mean/STD)
Control	0.56/0.19	0.56/0.18	0.55/0.17
CCM pre-resection group	0.32/0.15	0.38/0.12	0.4/0.14
p-value (ANOVA)	0.4	0.55	0.6

3.3. The default mode network (DMN) FC

Global network changes among the CCM subjects were also assessed using the DMN FC. In this ROI-based analysis, the MPFC was used as the seed and its connectivity to LPL, LPR and PCC was compared across groups, hence the DMN FC consists of three values. Shown in Fig. 9 and Table 9, there was a statistically significant decrease in the FC between MPFC and LPR among the CCM pre-resection group compared to the same value in the control group ($p = 0.00008$), whereas the differences in the FCs between MPFC and the other two DMN ROIs, i.e., LPL and PCC, were not statistically significant ($p = 0.35$ and 0.56, respectively). Interestingly, there is a statistically significant increase in the FCs between MPFC and LPR after surgical resection among the four CCM subjects compared to the same presurgical values ($p = 0.01$). Similar to what was observed in the analyses for the HFC and GFC, the surgical

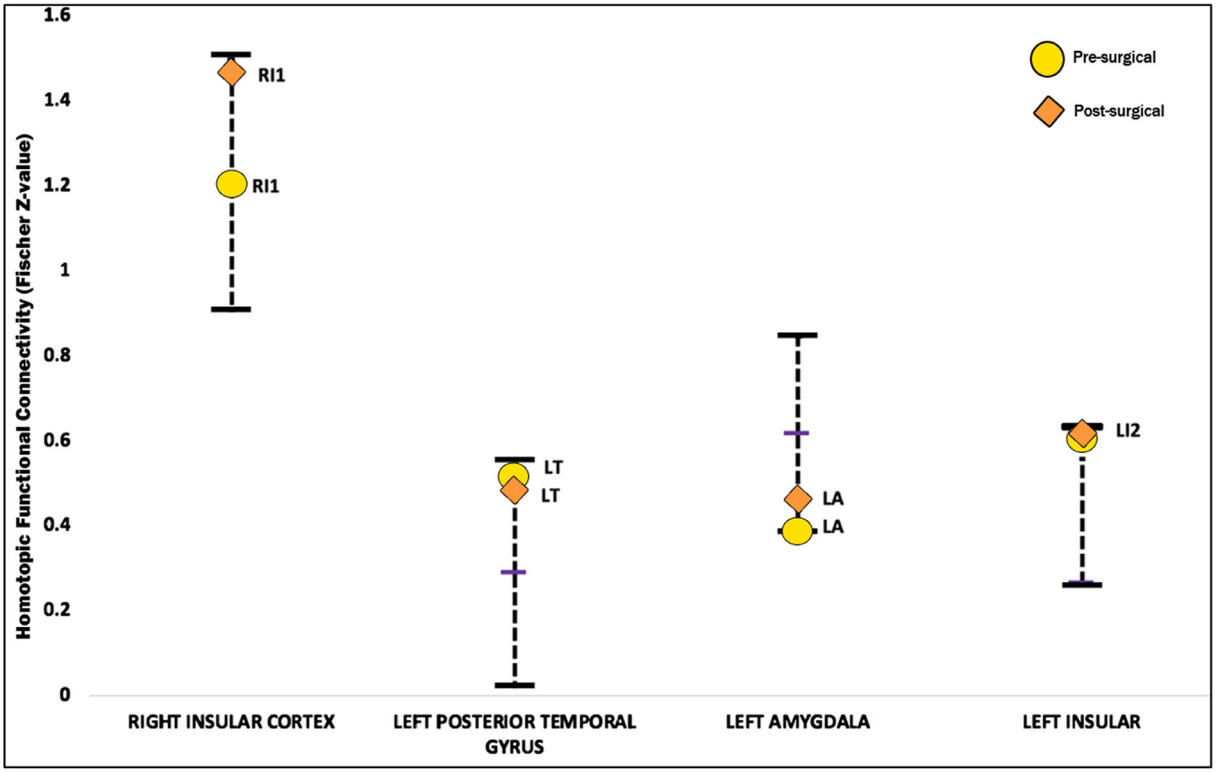

Fig. 4. The restoration of the disruption of the homotopic FC (HFC) in the CCM subjects after the surgical resection. Shown here are the pre-surgical (circle) and post-surgical (diamond) HFCs of each lesional ROI (labelled with the subject identifier) overlaid on the mean and the standard derivation of the HFC of the corresponding ROI estimated from the age- and gender-matched controls. Note that 3 (RI1, LA and LI2) out 4 subject showed increased HFC values after resection.

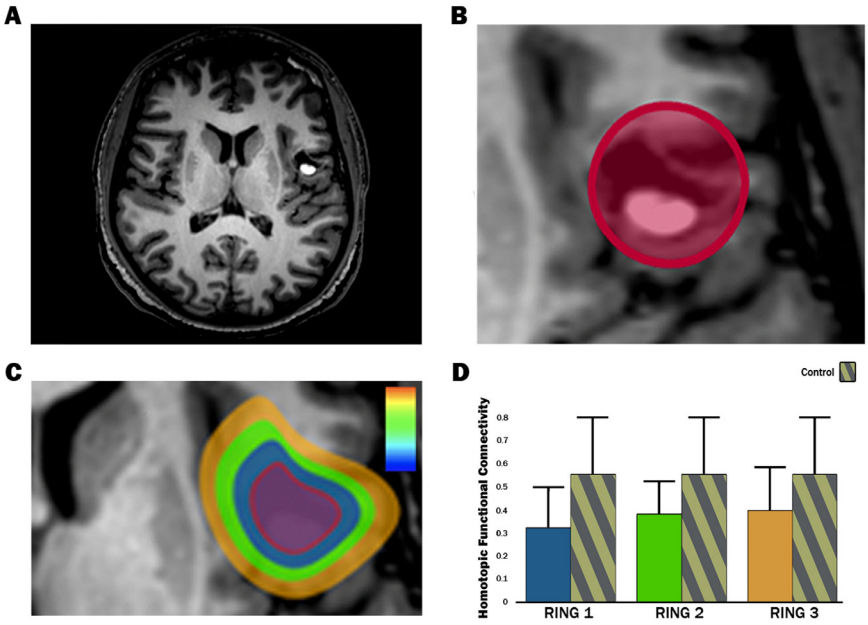

Fig. 5. The disruption of the HFC in the surrounding brain tissue of a CCM becomes less as its distance to the lesion increases. Shown here are the axial T1 images of an example of a CCM (subject LI2), (A) and (B). (C) shows the three rings used to delineate the surrounding brain tissue with its color corresponding to its mean HFC values. (D) shows the comparison of the mean and STD of HFC estimated from the lesional tissues with the same values estimated from the corresponding rings in the control group. Note that the HFCs from the lesional tissue are less than its control counterpart. Furthermore, the value of the HFC increases as the distance between the ring and the lesion increases, suggesting less disruption of the FC, (C) and (D).

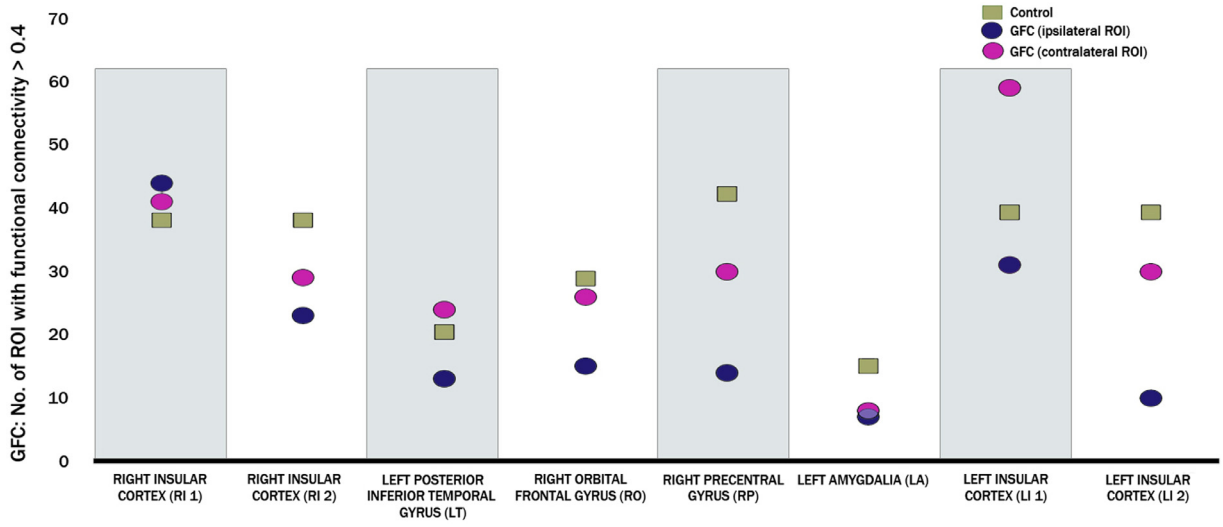

Fig. 6. The disruption of global FC (GFC) among the lesional ROIs. Shown here are the comparison between the global FC in the lesional ROIs (GFCipsilateral, blue circles) and its contralateral homotopic ROI (GPCcontralateral, purple circles) and the mean GFC estimated for the corresponding ROIs among the control group (green squares). Note that the GFCi are smaller in value compared to GFCc and those from the control group, suggesting the disruption of the GFCs for the lesional ROIs.

Table 6
The disruption of global FC (GFC) (number of ROIs) associated with the lesional ROIs.

ROI	GFCipsilateral	GFCcontralateral	Mean/std of GFC among Controls
RIGHT INSULAR CORTEX (RI1)	44	41	38/13.5
RIGHT INSULAR CORTEX (RI2)	23	29	Same as above
LEFT POSTERIOR INFERIOR TEMPORAL GYRUS (LT)	13	24	20/12.3
RIGHT ORBITAL FRONTAL GYRUS. (ROF)	15	26	28/16.7
RIGHT PRECENTRAL GYRUS (RPC)	14	30	42/18.2
LEFT AMYGDALA (LA)	7	8	15/10.7
LEFT INSULAR CORTEX (LI1)	31	59	39/11.5
LEFT INSULAR CORTEX (LI2)	10	30	Same as above

resection rendering the CCM subjects seizure free appeared to be associated with the restoration of the disruption of the normal FC.

Although, neither the FC of the MPFC and the LPL and the FC of the MPFC and PCC did not show a statistically significant difference between the controls, CCM group pre-resection and post-resection (control: $M = 0.42$, SD = 0.25, CCM group pre-resection: $M = 0.30$, SD = 0.18; $p = 0.14$), (CCM group pre-resection: $M = 0.30$, SD = 0.18; CCM group post-resection: $M = 0.41$, SD = 0.21; $p = 0.15$), there was a trend of decrease in these FC values in the CCM pre-resection group compared to controls and an increase after the resection of the CCM,

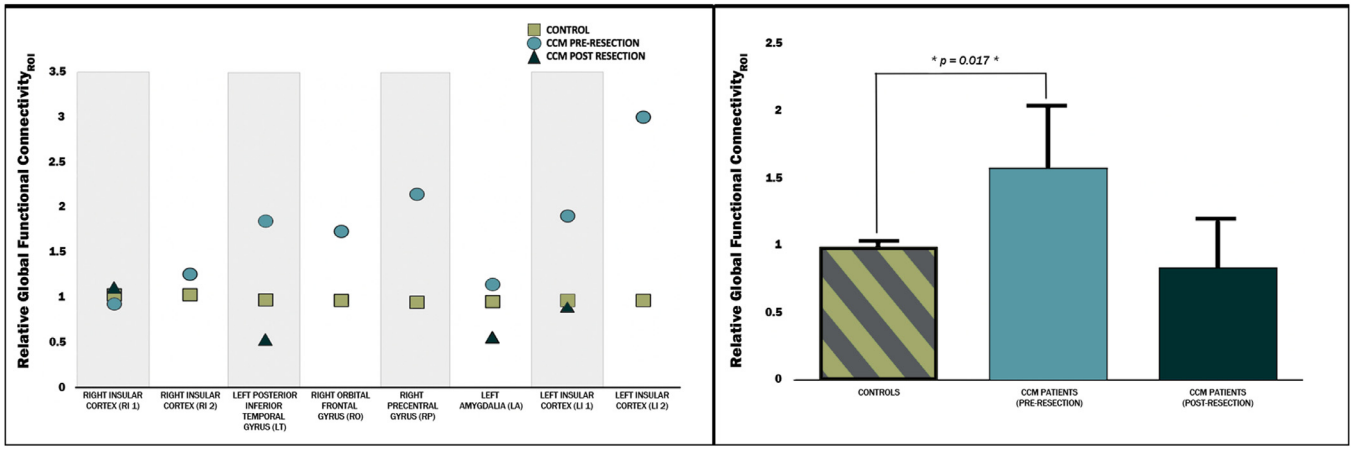

Fig. 7. The disruption of the global FC (GFC) among the lesional ROIs quantified using the $RGFC_{ROI}$ metric. The plot on the left shows that the lesional $RGFC_{ROI}$ values (blue circles) are greater than the control $RGFC_{ROI}$ (green squares), $p = 0.017$. Furthermore, three (LT, LA and LI1) of the 4 post-surgical lesional $RGFC_{ROI}$ (red triangles) showed decreased after the surgical resection compared to the pre-surgical value, $p = 0.2$. The plot on the right is the bar graph showing the same results. It appears that the lesion ROIs suffered the disruption of the GFC compared to the same ROIs in the control group and the surgical resection may help reverse the disruption.

Table 7
The disruption of the global FC (GFC) seen among the lesional ROIs quantified using the $RGFC_{ROI}$ metric.

	PRE-RESECTION)	POST –RESECTION	CONTROLS (mean/std)
RIGHT INSULAR CORTEX (RI1)	0.93	1.1	1.03/0.23
RIGHT INSULAR CORTEX (RI2)	1.26		Same as above
LEFT POSTERIOR INFERIOR TEMPORAL GYRUS (LT)	1.85	0.53	0.98/0.07
RIGHT ORBITAL FRONTAL GYRUS (ROF)	1.73		0.97/0.06
RIGHT PRECENTRAL GYRUS (RPC)	2.14		0.95/0.11
LEFT AMYGDALA (LA)	1.14	0.56	0.95/0.08
LEFT INSULAR CORTEX (LI1)	1.9	0.9	0.97/0.13
LEFT INSULAR CORTEX (LI2)	3		Same as above

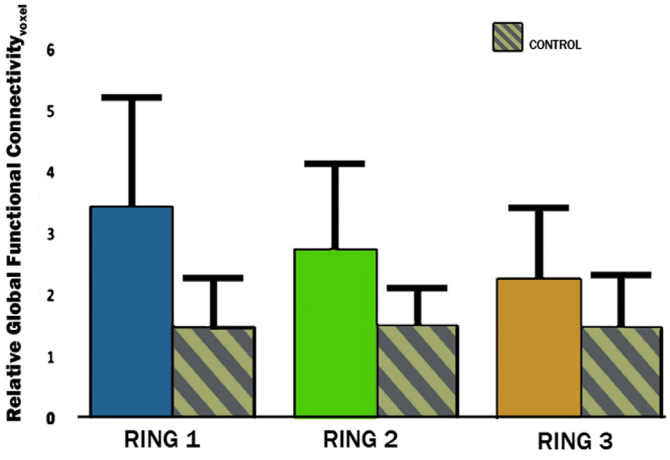

Fig. 8. The disruption of the GPC in the surrounding brain tissue of a CCM becomes less as its distance to the lesion increases. Shown here is the comparison of the mean and STD of $RGFC_{voxel}$ estimated from the lesional tissues with the same values estimated from the corresponding rings in the control group. Note that the $RGFC_{voxel}$ from the lesional tissue are larger than its control counterpart, i.e., the disruption of global FC associated with the CCM lesion. Furthermore, the value of the $RGFC_{voxel}$ decreases as the distance between the ring and the lesion increases, suggesting less disruption of the GFC.

Fig. 9 and Table 9.

Finally, we examined the effect of the laterality of the lesion on the DMN FC. Shown in Fig. 10 and Table 10 are the DMN FC in subjects with right and left hemisphere lesions compared to the control group. The statistically significant decrease in the FC between the MPFC and

Table 8
The voxel-based analysis on the RGFC changes in the surrounding brain tissue.

	Ring 1(mean/std)	Ring 2(mean/std)	Ring 3(mean/std)
Control	1.50/0.77	1.53/0.57	1.49/0.80
CCM pre-resection group	3.45/1.76	2.75/1.38	2.28/1.11
p-value (ANOVA)	0.7	0.5	0.4

the LPR among the CCM subjects compared to the control group were again observed in both subgroup analyses, i.e., the right-sided lesions and the left-sided lesions ($p = 0.00006$ and 0.03, respectively). In the subgroup analysis, the FC between the MPFC and LPL showed more decrease among the CCM subject with *left*-sided lesions compared to the control group than those with right-sided lesions, although neither comparison reached statistical significance. The connectivity of MPFC and PCC (midline ROI) did not seem to be affected by the laterality of the CCM location, Fig. 10 and Table 10.

4. Discussion

In this study, we compared the functional connectivity (FC) metrics estimated from resting state fMRI studies obtained from subjects with focal epilepsy caused by single cerebral cavernous malformation (CCM) and those from healthy age and gender matched controls. We showed that there was both regional and global disruption of the FC values among the CCM subjects including decreased in homotopic FC (HFC) and global FC (GFC) in the ROIs where the CCMs are located. There is also the disruption of the default mode network (DMN) especially the FC between MPFC and LPR among these individuals. We also observed the trend of alleviation of these disruption after the individual has

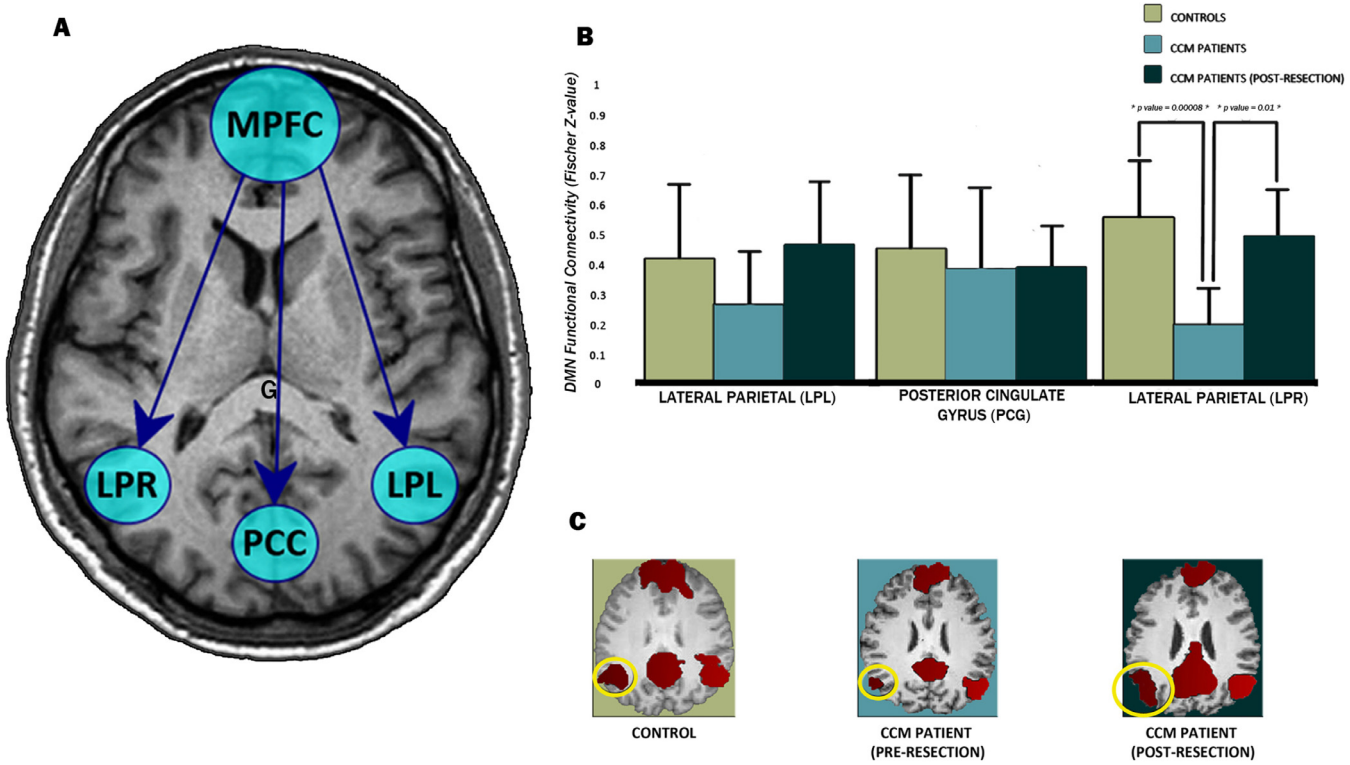

Fig. 9. The disruption of the FCs in default mode network (DMN) among the CCM subjects. Shown in (A) is the depiction of the ROIs involving DMN, MPFC, LPR, LPL and PCC. Using MPFC as the seed, the DMN FC consisted of the FC between MPFC and LPR, the FC between MPFC and LPL, and the FC between MPFC and PCC. (B) plots the mean and standard derivations of three values. With the left group are the FCs between MPFC and LPL, the middle, the FCs between MPFC and PCC and the right group, the FCs between MPFC and LPR. The green bars are the values from the control group, the light blue bars are the values from the pre-surgical CCM group, and the dark blue bars are the values from the post-surgical CCM group. Note that the DMN FCs among the CCM subjects were smaller in values in all three components compared to the controls, especially the FC between MPRC and LPR ($p = 0.00008$). Note that the DMN FCs among the 4 CCM subjects showed improvement in all three components after the surgical resection, especially the FC between MPRC and LPR ($p = 0.01$). The (C) plot are the coactivation maps for the DMN FCs for the control (left), pre-resection (middle) and post-resection (right) groups. Note LPR showed significant changes in the strength of coactivation among these three groups (circles).

Table 9
The disruption of the FCs in default mode network (DMN) among the CCM subjects.

GROUP	LPL(mean/std)	LPR (mean/std)	PCG (mean/std)
CONTROLS	0.42/0.25	0.55/0.19	0.45/0.24
CCM PRE-RESECTION	0.30/0.18	0.21/0.11	0.40/0.25
CCM POST-RESECTION	0.41/0.20	0.55/0.16	0.44/0.15

become seizure free from the surgical resection of the CCM. In addition, we found the disruption of the HFC and GFC in the brain tissue immediately adjacent to the CCM and it appears that the severity of the disruption is inversely proportional to the distance of the brain tissue to the lesion.

Epilepsy is a common neurological disorder affecting more than 1% of the general population and is associated with substantial morbidity and increased mortality (Wiebe, 2012). Although focal epilepsy such as the ones caused by lesions such as CCMs was historically considered a regional brain disorder associated with the epileptogenic zone (EZ) where the seizure originated. Growing evidence, however, pointed to wide brain network changes in focal epilepsy that extend beyond the EZ (Englot et al., 2015). Learning the structural and functional alterations of the brain network in focal epilepsy is essential in understanding the pathophysiology of the disease. The investigation of the brain network disturbance may help us characterize the network by which the seizure generates and prorogates. It can also help us understand the mechanism by which the recurrent seizure leads to cognitive and neuropsychological deficits. Furthermore, the impact of epilepsy on brain network influence the treatment outcomes of the disease, especially with the surgical treatment. It is a well known fact that the length of seizure history is inversely proportional to the rate of seizure freedom after the surgical intervention (Spencer et al., 2005). This is likely due to the complex and continuous alteration of brain network by the recurrent seizure.

Advanced MRI techniques have made it possible to probe the changes in neuronal networks *in vivo*. The MRI techniques can characterize both structural and functional network changes. Diffusion tensor images (DTIs) infer structural connectivity by identifying white matter fibers that physically connect two brain regions. Recent applications of DTI techniques have generated new understandings of pathophysiology of seizure disorders (Bandt et al., 2014; Liao et al., 2010). Vulliemoz et al. studied a cohort of 29 patients with juvenile myoclonic epilepsy (JME) using diffusion tensor imaging (DTI) and found alterations in microstructural connectivity of the mesial frontal region that may contribute to the onset of motor seizures in JME (Vulliemoz et al., 2011). Several studies conducted among patients with temporal lobe epilepsy (TLE) revealed structural connectivity alterations extending beyond the temporal lobes into both hemispheres independent of the seizure onset zone (Besson et al., 2014; DeSalvo et al., 2014; Pittau et al., 2012). These discoveries may help outline pathways of seizure propagation and functional deficits associated with TLE. For example, Li et al. studied the involvement of the cerebellum in idiopathic generalized epilepsy and showed the impairment of cerebellar fiber integrity among these patients (Li et al., 2010).

Functional connectivity abnormalities related to seizure disorders have been investigated with resting state fMRI (rsfMRI)

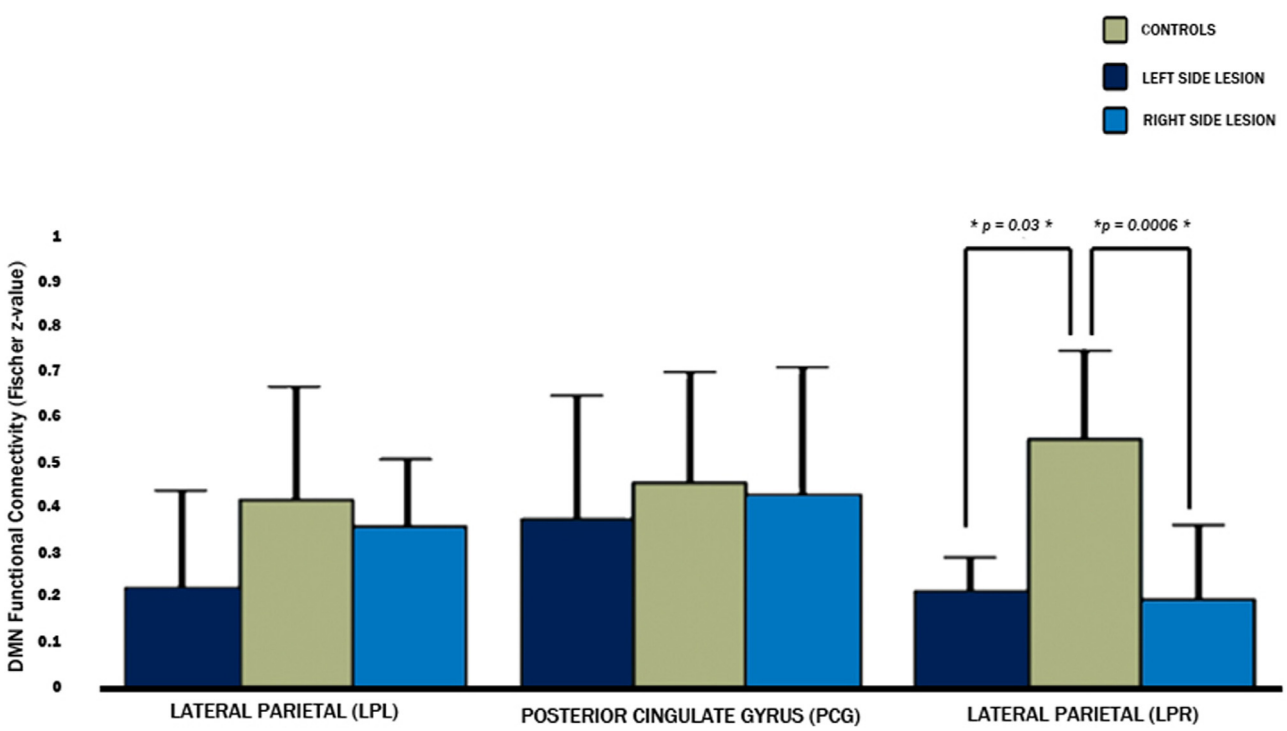

Fig. 10. The hemispheric location of the CCM influences the pattern of DMN FC disruption. The CCM subjects were divided into two groups depending on the hemispheric location of the CCM, left sided group (darker blue) and right sided group (lighter blue). The three DMN FC values from these two groups were compared with the control group (green). It appears that the disruption of the FC between MPRC and LPR remained statistically significant in the subgroup analysis (right plot). For the FC between MPFC and LPL, the disruption appeared worse when the lesion is on the left (dark blue) than when the lesion is on the right (light blue), left plot. The disruption to the FC between MPRC and PCC was least severe among the three FCs, middle plot.

Table 10
The hemispheric location of the CCM influences the pattern of DMN FC disruption.

GROUP	LPL (mean/std)	LPR (mean/std)	PCG (mean/std)
CONTROLS	0.42/0.25	0.56/0.19	0.45/0.24
LEFT-SIDED LESIONS	0.23/0.21	0.22/0.07	0.38/0.27
RIGHT-SIDED LESIONS	0.36/0.15	0.20/0.16	0.43/0.28

(Christiaen et al., 2019; Grassia et al., 2018; Liao et al., 2010; Morgan et al., 2019; Zhang et al., 2018, 2019). The majority of these studies have been conducted among patients with mesial temporal lobe epilepsy (MTLE). They have revealed that the amygdala and hippocampus ipsilateral to the seizure focus have decreased functional connectivity to the contralateral temporal lobe, ventromesial prefrontal region, as well as portions of the default mode network (DMN) (Haneef et al., 2012; Pittau et al., 2012).

To date, this is the first study where resting state functional connectivity abnormalities associated with focal epilepsy related to a single CCM were investigated. Our goal was to study the effect of focal epilepsy on the brain networks by applying a multi-resolution approach to investigate changes at the regional and global network levels. Our data showed that there was both regional and global disruption of the FC among the CCM subjects including decreased in homotopic FC (HFC) and global FC (GFC) in the regions of interest (ROIs) where the CCMs were located. There was also the disruption of the default mode network (DMN) especially the FC between the middle prefrontal cortex (MPFC) and the right lateral parietal cortex (LPR) among these individuals. The disruption of the normal functional connectivity can perhaps explain cognitive and psychological deficits observed on presurgical neuropsychological testing results among these individuals. Our data shows the trend of alleviation of these disruptions after the individual has become seizure free from the surgical resection of the CCM. This implies that the disruption of normal brain network may be reversible with the successful surgical treatment rendering the patient seizure free, although this trend will need to be confirmed with a larger study conhort. This reversibility of the function connectivity disruption was also observed by others in temporal lobe epilepsy (Morgan et al., 2019).

In addition, we found the disruption of the regional (HFC) and global (GFC) in the brain tissue immediately adjacent to the CCM and the severity of the disruption appeared inversely proportional to the distance of the brain tissue to the lesion. Even though these changes did not reach statistical significance in our analyses, they raised the possibility of using these values to delineate the epileptogenic zone (EZ) and, hence, to guide the surgical resection. The clinical experience has shown that the brain tissue surrounding the CCM lesion is most likely the epileptogenic zone in the CCM related focal epilepsy (Sevy et al., 2014). In order to render the patient seizure free, the surgical resection needs to remove the EZ. The exact boundary of EZ is however not well defined. Some neurosurgeons have used the discoloration from hemosiderin staining as an indication for the EZ, removing all the surrounding brain tissue with hemosiderin staining. Some other neurosurgeons employ intraoperative electrocorticography (ECOG) to guide the resection (Ferrier et al., 2007), resecting all the surrounding brain tissue until the ECOG shows no more epileptiform discharges. Both these strategies have limitations in defining the EZ associated with CCM. This is especially challenging if the CCM is located in the eloquent region of the brain. Our finding of the existence of a gradient in the degree of disruption in the FC value in the surrounding brain tissue points to the possibility of using this degree of the disruption to define the EZ. In order to do so, we need to continue our analysis by including a larger study cohorn so that this trend can be confirmed.

Another theory under consideration in epilepsy research is that seizures occur due to imbalances between excitatory and inhibitory neurotransmission (Buckmaster and Dudek, 1997; McCormick and

Contreras, 2001). In human and animal models of trauma-related epilepsy, the presence of spontaneous seizure is strongly associated with axon sprouting and reorganization of neural circuitry (Buckmaster et al., 2002). Many animal injury models show evidence that excitatory connectivity is enhanced and inhibitory influences are decreased. However, our CCM data suggests that the functional connectivity appears to be disrupted across global and regional networks. Functional connectivity is a direct measure of neuronal synchronization. Perhaps it is this decrease in normal neuronal synchronization that gives rise to an abnormal epileptic network and becomes a key element in the phenomenon of epileptogenesis.

4.1. Study limitations

The obvious limitation of this study is that this is a retrospective study on a small cohort of the subjects with single CCM ($n = 8$). This is largely due to the rarity of this condition. As a result of the small number of participants, several observations did not reach statistical significance. Even among the observations that reach statistical significance, the ability to apply these findings to other patients with similar conditions may be limited. Despite these limitations, this study nonetheless provides a unique approach to investigate the changes in brain networks associated with a type of focal epilepsy. The findings will need to be confirmed with much larger study cohorts.

5. Conclusion

In conclusion, using resting state functional MRI data, we showed that focal epilepsy caused by single cerebral cavernous malformation (CCM) is associated with the disruption of the normal regional and global functional connectivity (FC). The disruption included a decrease in the coactivation between the region surrounding the CCM lesion, i.e., the lesional region, and its homotopic counterpart, reduced FCs between the lesional region and the rest of the brain, and reduced FCs among the default mode network.

Declaration of Competing Interest

None.

Acknowledgement

This work was funded by Louisiana State University Health Science Center (LSUHSC) Grant-in-Aid 2018-2019, Project number 5493001038 Intramural Grant and LSUHSC M. Feist Seed Grant for young investigators. The authors would like to thank Ms. Deann Jewell, Mr. Cody Hanna, and Dr. James Clawson for the editorial and graphics assistance.

References

Aboitiz, F., Lopez, J., Montiel, J., 2003. Long distance communication in the human brain: timing constraints for inter-hemispheric synchrony and the origin of brain lateralization. Biol. Res. 36, 89–99.
Andrews-Hanna, J.R., Snyder, A.Z., Vincent, J.L., Lustig, C., Head, D., Raichle, M.E., Buckner, R.L., 2007. Disruption of large-scale brain systems in advanced aging. Neuron 56, 924–935.
Bandt, S.K., Bundy, D.T., Hawasli, A.H., Ayoub, K.W., Sharma, M., Hacker, C.D., Pahwa, M., Leuthardt, E.C., 2014. The role of resting state networks in focal neocortical seizures. PLoS ONE 9, e107401.
Bernasconi, A., 2017. Connectome-based models of the epileptogenic network: a step towards epileptomics? Brain 140, 2525–2527.
Bernhardt, B.C., Hong, S., Bernasconi, A., Bernasconi, N., 2013. Imaging structural and functional brain networks in temporal lobe epilepsy. Front. Hum. Neurosci. 7, 624.
Besson, P., Dinkelacker, V., Valabregue, R., Thivard, L., Leclerc, X., Baulac, M., Sammler, D., Colliot, O., Lehéricy, S., Samson, S., Dupont, S., 2014. Structural connectivity differences in left and right temporal lobe epilepsy. Neuroimage 100, 135–144.
Biswal, B., Yetkin, F.Z., Haughton, V.M., Hyde, J.S., 1995. Functional connectivity in the motor cortex of resting human brain using echo-planar MRI. Magn. Reson. Med. 34, 537–541.
Buckmaster, P.S., Dudek, F.E., 1997. Network properties of the dentate gyrus in epileptic rats with hilar neuron loss and granule cell axon reorganization. J. Neurophysiol. 77, 2685–2696.
Buckmaster, P.S., Zhang, G.F., Yamawaki, R., 2002. Axon sprouting in a model of temporal lobe epilepsy creates a predominantly excitatory feedback circuit. J. Neurosci. 22, 6650–6658.
Buckner, R.L., Andrews-Hanna, J.R., Schacter, D.L., 2008. The brain's default network: anatomy, function, and relevance to disease. Ann. N.Y. Acad. Sci. 1124, 1–38.
Christiaen, E., Goossens, M.G., Raedt, R., Descamps, B., Larsen, L.E., Craey, E., Carrette, E., Vonck, K., Boon, P., Vanhove, C., 2019. Alterations in the functional brain network in a rat model of epileptogenesis: a longitudinal resting state fMRI study. Neuroimage, 116144.
Cordes, D., Haughton, V.M., Arfanakis, K., Wendt, G.J., Turski, P.A., Moritz, C.H., Quigley, M.A., Meyerand, M.E., 2000. Mapping functionally related regions of brain with functional connectivity MR imaging. AJNR Am. J. Neuroradiol. 21, 1636–1644.
Cox, R.W., 1996. AFNI: software for analysis and visualization of functional magnetic resonance neuroimages. Comput. Biomed. Res. 29, 162–173.
de Tisi, J., Bell, G.S., Peacock, J.L., McEvoy, A.W., Harkness, W.F., Sander, J.W., Duncan, J.S., 2011. The long-term outcome of adult epilepsy surgery, patterns of seizure remission, and relapse: a cohort study. Lancet 378, 1388–1395.
DeSalvo, M.N., Douw, L., Tanaka, N., Reinsberger, C., Stufflebeam, S.M., 2014. Altered structural connectome in temporal lobe epilepsy. Radiology 270, 842–848.
Dillon, W.P., 1997. Cryptic vascular malformations: controversies in terminology, diagnosis, pathophysiology, and treatment. AJNR Am. J. Neuroradiol. 18, 1839–1846.
Duffy, F.H., McAnulty, G.B., Albert, M.S., 1996. Effects of age upon interhemispheric EEG coherence in normal adults. Neurobiol. Aging. 17, 587–599.
Englot, D.J., Hinkley, L.B., Kort, N.S., Imber, B.S., Mizuiri, D., Honma, S.M., Findlay, A.M., Garrett, C., Cheung, P.L., Mantle, M., Tarapore, P.E., Knowlton, R.C., Chang, E.F., Kirsch, H.E., Nagarajan, S.S., 2015. Global and regional functional connectivity maps of neural oscillations in focal epilepsy. Brain 138, 2249–2262.
Englot, D.J., Konrad, P.E., Morgan, V.L., 2016. Regional and global connectivity disturbances in focal epilepsy, related neurocognitive sequelae, and potential mechanistic underpinnings. Epilepsia 57, 1546–1557.
Ferrier, C.H., Aronica, E., Leijten, F.S., Spliet, W.G., Boer, K., van Rijen, P.C., van Huffelen, A.C., 2007. Electrocorticography discharge patterns in patients with a cavernous hemangioma and pharmacoresistent epilepsy. J. Neurosurg. 107, 495–503.
Fransson, P., 2005. Spontaneous low-frequency BOLD signal fluctuations: an fMRI investigation of the resting-state default mode of brain function hypothesis. Hum. Brain Mapp. 26, 15–29.
Grassia, F., Poliakov, A.V., Poliachik, S.L., Casimo, K., Friedman, S.D., Shurtleff, H., Giussani, C., Novotny, E.J., Ojemann, J.G., Hauptman, J.S., 2018. Changes in resting-state connectivity in pediatric temporal lobe epilepsy. J. Neurosurg. Pediatr. 22, 270–275.
Gusnard, D.A., Akbudak, E., Shulman, G.L., Raichle, M.E., 2001. Medial prefrontal cortex and self-referential mental activity: relation to a default mode of brain function. Proc. Natl. Acad. Sci. USA 98, 4259–4264.
Hagmann, P., Thiran, J.P., Jonasson, L., Vandergheynst, P., Clarke, S., Maeder, P., Meuli, R., 2003. DTI mapping of human brain connectivity: statistical fibre tracking and virtual dissection. Neuroimage 19, 545–554.
Hamilton, J.P., Farmer, M., Fogelman, P., Gotlib, I.H., 2015. Depressive rumination, the default-mode network, and the dark matter of clinical neuroscience. Biol. Psychiatry 78, 224–230.
Haneef, Z., Lenartowicz, A., Yeh, H.J., Engel, J., Stern, J.M., 2012. Effect of lateralized temporal lobe epilepsy on the default mode network. Epilepsy Behav. 25, 350–357.
Innocenti, G.M., Aggoun-Zouaoui, D., Lehmann, P., 1995. Cellular aspects of callosal connections and their development. Neuropsychologia 33, 961–987.
Jette, N., Wiebe, S., 2013. Update on the surgical treatment of epilepsy. Curr. Opin. Neurol. 26, 201–207.
Kramer, M.A., Cash, S.S., 2012. Epilepsy as a disorder of cortical network organization. Neuroscientist 18, 360–372.
Larson-Prior, L.J., Zempel, J.M., Nolan, T.S., Prior, F.W., Snyder, A.Z., Raichle, M.E., 2009. Cortical network functional connectivity in the descent to sleep. Proc. Natl. Acad. Sci. USA 106, 4489–4494.
Le Bihan, D., Mangin, J.F., Poupon, C., Clark, C.A., Pappata, S., Molko, N., Chabriat, H., 2001. Diffusion tensor imaging: concepts and applications. J. Magn. Reson. Imaging 13, 534–546.
Li, Y., Du, H., Xie, B., Wu, N., Wang, J., Wu, G., Feng, H., Jiang, T., 2010. Cerebellum abnormalities in idiopathic generalized epilepsy with generalized tonic-clonic seizures revealed by diffusion tensor imaging. PLoS ONE 5, e15219.
Liao, W., Zhang, Z., Pan, Z., Mantini, D., Ding, J., Duan, X., Luo, C., Lu, G., Chen, H., 2010. Altered functional connectivity and small-world in mesial temporal lobe epilepsy. PLoS ONE 5, e8525.
Lowe, M.J., Dzemidzic, M., Lurito, J.T., Mathews, V.P., Phillips, M.D., 2000. Correlations in low-frequency BOLD fluctuations reflect cortico-cortical connections. Neuroimage 12, 582–587.
McCormick, D.A., Contreras, D., 2001. On the cellular and network bases of epileptic seizures. Annu. Rev. Physiol. 63, 815–846.
Moeller, F., Maneshi, M., Pittau, F., Gholipour, T., Bellec, P., Dubeau, F., Grova, C., Gotman, J., 2011. Functional connectivity in patients with idiopathic generalized epilepsy. Epilepsia 52, 515–522.
Mohammed, H.S., Kaufman, C.B., Limbrick, D.D., Steger-May, K., Grubb, R.L., Rothman, S.M., Weisenberg, J.L., Munro, R., Smyth, M.D., 2012. Impact of epilepsy surgery on seizure control and quality of life: a 26-year follow-up study. Epilepsia 53, 712–720.
Morgan, V.L., Rogers, B.P., Gonzalez, H.F.J., Goodale, S.E., Englot, D.J., 2019. Characterization of postsurgical functional connectivity changes in temporal lobe epilepsy. J. Neurosurg. 1–11.

Mulders, P.C., van Eijndhoven, P.F., Schene, A.H., Beckmann, C.F., Tendolkar, I., 2015. Resting-state functional connectivity in major depressive disorder: a review. Neurosci. Biobehav. Rev. 56, 330–344.
Pittau, F., Grova, C., Moeller, F., Dubeau, F., Gotman, J., 2012. Patterns of altered functional connectivity in mesial temporal lobe epilepsy. Epilepsia 53, 1013–1023.
Raichle, M.E., MacLeod, A.M., Snyder, A.Z., Powers, W.J., Gusnard, D.A., Shulman, G.L., 2001. A default mode of brain function. Proc. Natl. Acad. Sci. USA 98, 676–682.
Robinson, J.R., Awad, I.A., Little, J.R., 1991. Natural history of the cavernous angioma. J. Neurosurg. 75, 709–714.
Salvador, R., Martinez, A., Pomarol-Clotet, E., Sarro, S., Suckling, J., Bullmore, E., 2007. Frequency based mutual information measures between clusters of brain regions in functional magnetic resonance imaging. Neuroimage 35, 83–88.
Sevy, A., Gavaret, M., Trebuchon, A., Vaugier, L., Wendling, F., Carron, R., Regis, J., Chauvel, P., Gonigal, A.M., Bartolomei, F., 2014. Beyond the lesion: the epileptogenic networks around cavernous angiomas. Epilepsy Res. 108, 701–708.
Simard, J.M., Garcia-Bengochea, F., Ballinger, W.E., Mickle, J.P., Quisling, R.G., 1986. Cavernous angioma: a review of 126 collected and 12 new clinical cases. Neurosurgery 18, 162–172.
Spencer, S.S., Berg, A.T., Vickrey, B.G., Sperling, M.R., Bazil, C.W., Shinnar, S., Langfitt, J.T., Walczak, T.S., Pacia, S.V., Surgery, M.S.o.E., 2005. Predicting long-term seizure outcome after resective epilepsy surgery: the multicenter study. Neurology 65, 912–918.
Stark, D.E., Margulies, D.S., Shehzad, Z.E., Reiss, P., Kelly, A.M., Uddin, L.Q., Gee, D.G., Roy, A.K., Banich, M.T., Castellanos, F.X., Milham, M.P., 2008. Regional variation in interhemispheric coordination of intrinsic hemodynamic fluctuations. J. Neurosci. 28, 13754–13764.
Steiger, H.J., Markwalder, T.M., Reulen, H.J., 1987. Clinicopathological relations of cerebral cavernous angiomas: observations in eleven cases. Neurosurgery 21, 879–884.
Sze, G., Krol, G., Olsen, W.L., Harper, P.S., Galicich, J.H., Heier, L.A., Zimmerman, R.D., Deck, M.D., 1987. Hemorrhagic neoplasms: MR mimics of occult vascular malformations. AJR Am. J. Roentgenol. 149, 1223–1230.
Toro, R., Fox, P.T., Paus, T., 2008. Functional coactivation map of the human brain. Cereb Cortex 18, 2553–2559.
van den Heuvel, M.P., Hulshoff Pol, H.E., 2010. Exploring the brain network: a review on resting-state fMRI functional connectivity. Eur. Neuropsychopharmacol. 20, 519–534.
Verche, E., San Luis, C., Hernandez, S., 2018. Neuropsychology of frontal lobe epilepsy in children and adults: systematic review and meta-analysis. Epilepsy Behav. 88, 15–20.
Vulliemoz, S., Vollmar, C., Koepp, M.J., Yogarajah, M., O'Muircheartaigh, J., Carmichael, D.W., Stretton, J., Richardson, M.P., Symms, M.R., Duncan, J.S., 2011. Connectivity of the supplementary motor area in juvenile myoclonic epilepsy and frontal lobe epilepsy. Epilepsia 52, 507–514.
Weaver, K.E., Poliakov, A., Novotny, E.J., Olson, J.D., Grabowski, T.J., Ojemann, J.G., 2018. Electrocorticography and the early maturation of high-frequency suppression within the default mode network. J. Neurosurg. Pediatr. 21, 133–140.
Wiebe, S., 2012. Epilepsy. Outcome patterns in epilepsy surgery–the long-term view. Nat. Rev. Neurol. 8, 123–124.
Zhang, C., Yang, H., Liu, C., Zhang, G., Chen, N., Li, K., 2018. Brain network alterations of mesial temporal lobe epilepsy with cognitive dysfunction following anterior temporal lobectomy. Epilepsy Behav. 87, 123–130.
Zhang, C., Zhang, H., Xu, K., Yang, H., Liu, C., Yu, T., Chen, N., Li, K., 2019. Impaired prefrontal cortex-thalamus pathway in intractable temporal lobe epilepsy with aberrant executive control function: MRI evidence. Clin. Neurophysiol. 130, 484–490.